An Analytical Approach to the Nonlinear Dynamics of Moist Frontogenesis

FABIO CASTELLI

Istituto di Idraulica, Facoltà di Ingegneria, Universita' degli Studi di Perugia, Perugia, Italy

RAFAEL L. BRAS

Ralph M. Parsons Laboratory for Water Resources and Hydrodynamics, Massachusetts Institute of Technology, Cambridge, Massachusetts

KERRY A. EMANUEL

Center for Meteorology and Physical Oceanography, Massachusetts Institute of Technology, Cambridge, Massachusetts

(Manuscript received 15 July 1991, in final form 3 August 1992)

ABSTRACT

The existence of analytical solutions for two-dimensional nonlinear semigeostrophic models of moist frontogenesis is investigated. Two different schemes for the modeling of stratiform cloud thermodynamics are taken into account, one based on the assumption of an everywhere cloudy environment, while in the other the atmosphere is considered to be exactly saturated and only condensation effects are relevant. In the first case, an exact analytical solution is derived for arbitrary boundary conditions, which satisfies the requirements for the validation of the semigeostrophic approximation even when the atmosphere is conditionally unstable with respect to slantwise convection. The growth of symmetric instabilities with no short-wave cutoff is predicted for this conditionally unstable atmosphere, even under the approximations of the semigeostrophic theory. An analogous, but approximate, analytical solution is then proposed for the second case. The errors introduced by the approximation are, however, not bigger than the terms neglected in the semigeostrophic approximation itself.

1. Introduction

A major breakthrough in the study of frontogenesis was the introduction of semigeostrophic theory by Hoskins and Bretherton (1972). In an ideal dry-adiabatic atmosphere (linear problem for suitable initial conditions) semigeostrophic theory explains many fluid-dynamical aspects of front formation (Hoskins 1982). Some limits of the dry frontogenesis models have nevertheless been highlighted during the years, in particular those related to the thermodynamic aspects of the problem (Emanuel 1985). As an example, one of the major discrepancies, evident when the dry atmosphere solutions are compared with observed fronts, is in the distribution of the vertical velocities (Blumen 1980; Ogura and Portis 1982). Also, the role of the diabatic heating due to cloud condensation becomes crucial in the study of the interaction between frontal circulation and conditional symmetric instabilities (Bennets and Sharp 1982; Emanuel 1983; Xu 1989). Because of the progressive scale contraction mechanism in the cross-front direction, a close interaction is expected between the frontal circulation and mesoscale instabilities. Analytical approaches to the investigation of such a problem, based on perturbation analyses of the primitive equations, require the formulation of an analytical solution for the undisturbed base-state circulation.

If the inviscid primitive equations are expanded in series of a small Rossby number in the cross-front direction, the resulting zero-order approximation leads to the formulation of the semigeostrophic theory of frontogenesis. Higher-order approximations to the solution of the frontal circulation may be then obtained if a solution of the zero-order problem is known in closed form. When the effects of heat release due to cloud condensation are taken into account, even the application of the semigeostrophic theory leads to a nonlinear set of partial differential equations, which have been solved numerically (Thorpe and Emanuel 1985; Joly and Thorpe 1989). The existence of possible analytical solutions and the derivation techniques are the main objects of the present work. This will provide a better insight into the dynamics of moist frontogenesis and also serve as a preliminary step toward the investigation of the interaction between frontal circulation and symmetric instabilities.

Corresponding author address: Dr. Rafael L. Bras, Ralph M. Parsons Laboratory, Massachusetts Institute of Technology, Department of Civil and Environmental Engineering, Cambridge, MA 02139.

Two types of nonlinear behavior are evident in the formulation of the model under investigation: the first one, strictly connected with the eventual evolution of symmetric instabilities, depends on the evolution of the potential vorticity field, otherwise conserved in a dry atmosphere; the second one, of threshold type, is due to the different roles played by the water vapor condensation and cloud evaporation processes. Two different simplified schemes are studied in order to analyze and compare the relevance of the two nonlinearities. The two schemes are based on different hypotheses about the distribution of the cloudy areas in the domain. If a "moist-up–moist-down" assumption is made and the atmosphere is considered to contain suspended liquid water everywhere, with both condensation and evaporation effects, an exact particular analytical solution can be obtained. This solution satisfies the requirements of the semigeostrophic approximation also in an atmosphere that is conditionally unstable with respect to slantwise convection. A similar, but approximate, analytical solution is also proposed for the "moist-up–dry-down" scheme first investigated numerically in Thorpe and Emanuel (1985). The order of approximation of such a particular solution is found to be not bigger than the order of magnitude of the semigeostrophic approximation itself.

2. A semigeostrophic model of moist frontogenesis

The semigeostrophic dynamics of frontogenesis, as driven by a synoptic-scale horizontal deformation field, can be described by the set of partial differential equations (Hoskins and Bretherton 1972)

$$Q_T - AXQ_X - \frac{\Xi}{fr}\Psi_X Q_Z = \frac{\Xi}{r} S_Z, \tag{1}$$

$$f^2\left(\frac{1}{r}\Psi_Z\right)_Z + \frac{g}{f\Theta_0}(Q\Psi_X)_X = -\frac{g}{\Theta_0} S_X - 2A\Phi_{XZ}, \tag{2}$$

$$\frac{1}{f^2}\Phi_{XX} + \frac{f\Theta_0}{grQ}\Phi_{ZZ} = 1, \tag{3}$$

defined in a cross-front symmetry plane in semigeostrophic coordinates $(X, Z, T) = (x + \Phi_X/f^2, z, t) \in (-\infty, +\infty) \times (0, H) \times (-\infty, T_0)$, bounded by the earth surface and the tropopause, both considered as rigid plates.

The unknowns taken in the above system of equations are the geopotential Φ, the ageostrophic streamfunction Ψ, and the Ertel's potential vorticity Q (defined in terms of potential temperature). The constant Coriolis parameter f, the reference potential temperature Θ_0, and a geostrophic deformation forcing $A(T)$ are considered as given parameters for the problem. A pseudodensity of the air, r, may be considered constant as well in a Boussinesq approximation.

The vertical component of the absolute vorticity Ξ and the diabatic heating source S are expressed as explicit functions of the unknown fields Φ and Ψ. In particular Ξ can be written in the form:

$$\Xi = \frac{f}{1 - (1/f^2)\Phi_{XX}}. \tag{4}$$

The time of front formation, T_0, may be defined as the time when the vertical component of the absolute vorticity becomes singular, that is, when $\Phi_{XX}(X', Z', T_0) = f^2$ at some point (X', Z').

Assuming that condensation is the only relevant diabatic process at the spatial and temporal scales of the given problem, and also that the major contribution to the change of specific humidity following a fluid particle is due to the vertical advection along $X = \text{const}$ surfaces in updraft regions (negative Ψ_X), the heating source can be expressed as (Thorpe and Emanuel 1985):

$$S = \frac{1}{f}\left(\frac{\Gamma_m}{\Gamma_d} Q_e - Q\right) F(\Psi_X); \tag{5}$$

Q_e is a potential vorticity defined in terms of equivalent potential temperature, which, by means of Ertel's theorem, is considered as a given constant throughout all the domain of integration. In (5) Γ_m/Γ_d is the ratio between the moist and the dry adiabatic lapse rates of temperature. (This last term was mistakenly missed in the original formulation of the model, and subsequently introduced in Emanuel and Fantini (1987).]

To study the effect of the diabatic heat exchange on the frontal circulation, two simplified schemes can be adopted:

- a "moist-up–dry-down" (MUDD) scheme ($F(\Psi_X) = \Psi_X H(-\Psi_X)$), where an everywhere saturated atmosphere is considered, such that condensation of water vapor is present wherever the updraft velocity is positive; condensed water is assumed to precipitate immediately, so that evaporation of clouds is completely neglected; $H(\cdot)$ is the Heaviside step function, defined as $H(x) = 0$ if $x \leq 0$ and $H(x) = 1$ if $x > 0$;
- a "moist-up–moist-down" (MUMD) scheme ($F(\Psi_X) = \Psi_X$), where an everywhere cloudy atmosphere is considered, with both condensation (updraft velocity) and evaporation (downdraft velocity).

Both schemes are very crude simplifications of the moisture distribution in the real atmosphere. The first one does not allow for the presence of any cloud. The second one is not representative of the usually observed difference in the average absolute humidity between the cold descending and the warm ascending air masses. Even if the MUMD scheme may be considered the weakest approximation, it allows, due to its simpler mathematical formulation, for a more complete investigation of some of the basic effects of the diabatic heat exchange on the frontal circulation. The MUMD case will also permit some preliminary conclusions of the behavior of undisturbed semigeostrophic solutions

in an atmosphere that is unstable with respect to moist slantwise convection, and on their interaction with growing symmetric instabilities.

The boundary conditions are null vertical velocity and given potential temperature profiles $(\Theta_0/g)\Phi_Z$ on the horizontal boundaries. All the horizontal gradients and ageostrophic velocities at infinite distance from the center of the domain vanish (given no vertical velocity on the horizontal boundaries, the potential temperature profiles are fixed there at any time in the stretched coordinate βX, where $\beta = \exp \int_{t_0}^{t} A(\eta)d\eta$):

$$\Phi_Z(X, 0, T) = \Theta_b(\beta X), \quad \lim_{X\to\pm\infty} \Theta_{b,X} = 0, \tag{6}$$

$$\Phi_Z(X, H, T) = \Theta_b(\beta X) + \frac{grHQ_0}{\Theta_0 f}, \tag{7}$$

$$\lim_{X\to\pm\infty} \Phi = \left(Z - \frac{H}{2}\right)\Theta_b(\beta X) + \frac{grZ^2Q_0}{2\Theta_0 f}, \tag{8}$$

$$\Psi(X, 0, T) = \Psi(X, H, T) = 0, \tag{9}$$

$$\lim_{X\to\pm\infty} \Psi = \lim_{X\to\pm\infty} \Psi_X = \cdots = \lim_{X\to\pm\infty} \Psi_{X\cdots X} = 0, \tag{10}$$

where Q_0 is a reference potential vorticity corresponding to the initial condition for an undisturbed atmosphere back in the past:

$$\lim_{T\to-\infty} Q(X, Z, T) = Q_0. \tag{11}$$

To look for a suitable nondimensional form of the problem, we choose the following nondimensional variables (lowercase), assuming a pseudo Brunt–Väisällä frequency $N = [(grQ_0)/(\Theta_0 f)]^{1/2}$, in the Boussinesq approximation:

TABLE 1. Typical values of the various atmospheric parameters at the midlatitude, and derived reference magnitude for the various variables used in the model. U, V, and W are the horizontal cross-front, horizontal longfront, and vertical components of the wind velocity. The reference magnitude of some of the variables varies in time according to the contraction parameter β.

Parameter		Variables (dimensional)	
N	10^{-2} s^{-1}	X	$10^6/\beta$ m
		Z	10^4 m
H	10^4 m	T	10^5 s (27.78 hours)
		Q	2×10^{-7} m^2 s^{-1} °K kg^{-1}
f	10^{-4} s^{-1}	Q_e	4×10^{-7} m^2 s^{-1} °K kg^{-1}
		Ξ	10^{-4} s^{-1}
A_0	10^{-5} s^{-1}	S	2×10^{-4} °K s^{-1}
		Ψ	10^5 kg m^{-1} s^{-1}
r_0	1 kg m^{-3}	Φ	10^4 m^2 s^{-2}
		Θ_b	20°K
Q_0	2×10^{-7} m^2 s^{-1} °K kg^{-1}	U	10 m s^{-1}
		V	β 100 m s^{-1}
Γ_m/Γ_d	0.5	W	β 10^{-1} m s^{-1}

$$Z = H\left(z + \frac{1}{2}\right); \quad X = \frac{NH}{f\beta}x; \quad T = \frac{t}{A_0};$$

$$A = A_0\alpha; \quad Q = Q_0 q; \quad \frac{\Gamma_m}{\Gamma_d}Q_e = Q_0 q_e;$$

$$S = \frac{Q_0 H A_0 r}{f}s; \quad \Psi = \frac{NH^2 A_0 r}{f}\psi; \quad \Phi = N^2H^2\phi;$$

$$\Xi = f\xi; \quad \Theta_b = \frac{HrQ_0}{f}\theta_b.$$

In order to obtain a dimensional interpretation of the results discussed later on, the values reported in Table 1 for the various parameters can be assumed. The reference magnitude for the various variables, derived using such typical values for the parameters, are also reported in the same table.

Assuming that the potential and absolute vorticities remain positive and finite, the following set of equations in the unknowns (q, f, ψ) is obtained:

$$(1 - \beta^2\phi_{xx})q_t + \beta(q - q_e)\psi_{xz}(1 - G(\psi_x)) - \beta q_z\psi_x G(\psi_x) = 0, \tag{12}$$

$$\psi_{zz} + (q_e + (1 - q_e)G(\psi_x))\beta^2\psi_{xx} + 2\alpha\beta\phi_{xz} = 0, \tag{13}$$

$$\phi_{zz} - (1 - \beta^2\phi_{xx})q = 0, \tag{14}$$

where

$$G(\psi_x) = \begin{cases} H(\psi_x), & \text{moist up/dry down} \\ 0, & \text{moist up/moist down,} \end{cases} \tag{15}$$

with boundary and initial conditions:

$$\phi_z\left(x, -\frac{1}{2}, t\right) = \theta_b(x), \quad \lim_{x\to\pm\infty} \theta_{bx} = 0, \tag{16}$$

$$\phi_z\left(x, \frac{1}{2}, t\right) = \theta_b(x) + 1, \tag{17}$$

$$\lim_{x\to\pm\infty} \phi = z\theta_b(x) + \frac{\left(z + \frac{1}{2}\right)^2}{2}, \tag{18}$$

$$\psi\left(x, -\frac{1}{2}, t\right) = \psi\left(x, \frac{1}{2}, t\right) = 0, \tag{19}$$

$$\lim_{x\to\pm\infty} \psi = \lim_{x\to\pm\infty} \psi_X = \cdots = \lim_{x\to\pm\infty} \psi_{X\cdots X} = 0, \tag{20}$$

$$\lim_{t\to-\infty} q(x, z, t) = 1. \tag{21}$$

The semigeostrophic approximation is valid if the cross-front inertial terms are small relative to the longfront geostrophic velocity multiplied by the Coriolis parameter. The validity of the inviscid approximation

depends on the magnitude of the Richardson number, which must be $>1/10$. These two conditions can be stated as (Hoskins and Bretherton 1972):

$$|u_t + wu_z| = |(\beta^2\xi\phi_{xz}\psi_x + \psi_z)_t - \beta\xi\psi_x(\beta^2\xi\phi_{xz}\psi_x + \psi_z)_z| \ll \frac{f^2}{A_0^2}|v_g| = \frac{f^2}{A_0^2}|\beta\phi_x|, \quad (22)$$

$$|\xi| = \left|\frac{1}{1-\beta^2\phi_{xx}}\right| \leqslant 10, \quad (23)$$

where u and w are the horizontal and vertical components of the nondimensional ageostrophic velocity, v_g is the long-front dimensional geostrophic velocity, and the Rossby number $\mathrm{Ro} = A_0/f$ is usually of the order of 10^{-1}.

Two different sources of nonlinearity are present in the set of Eqs. (12)–(14), namely, the dependence of the ellipticity coefficient G on the sign of ψ_x (in the MUDD scheme) and the products between q and ϕ_{xx} and ψ_{xz}. In a dry atmosphere, that is, $q_e = 1$ and $G = 0$, the potential vorticity field remains constant at any time and the problem becomes linear.

3. Formulation of a particular analytical solution

If the moist frontogenesis is assumed to take place in an atmosphere that is stable with respect to dry slantwise convection, that is, the potential vorticity q is positive everywhere, Eq. (14) can be inverted to obtain the potential vorticity q itself. Substitution into (12) reduces the problem to a set of two equations with unknowns (ϕ, ψ):

$$\{\phi_{zzt} - q_e(1 - G(\psi_x))\beta\psi_{xz} - G(\psi_x)\beta\xi\phi_{zzz}\psi_x\} \times (1 - \beta^2\phi_{xx}) + \phi_{zz}\{(\beta^2\phi_{xx})_t + (1 - G(\psi_x))\beta\psi_{xz} - G(\psi_x)\beta^3\xi\phi_{xxz}\psi_x\} = 0, \quad (24)$$

$$\psi_{zz} + (q_e + (1 - q_e)G(\psi_x))\beta^2\psi_{xx} + 2\alpha\beta\phi_{xz} = 0. \quad (25)$$

An exact particular solution to such a highly nonlinear problem can be obtained in the MUMD case if it is assumed that the potential vorticity is uniform in the initial condition.

In the MUDD case, it might be assumed that the potential vorticity remains uniform in the downdraft areas [according to the classical dry scheme, Eq. (12) is "locally" homogeneous in q if $\psi_x \geqslant 0$] and that the potential vorticity evolves in the updraft areas according to the moist scheme. In reality, the interface between updraft and downdraft areas will tend to move toward the warm (updraft) side (as shown later). The dry scheme is then to be applied, as the time integration of the equations proceeds, also to areas where the potential vorticity, having previously experienced the moist evolution, is no longer uniform. In order to solve the MUDD case we will assume that this last mentioned effect is negligible, and will approximate the potential vorticity to be uniform in the whole downdraft area at any time. The validity of this approximation will be shown later. Then a particular solution to both schemes (exact in the MUMD case, approximated in the MUDD one) can be obtained studying the reduced system (whose derivation is given in appendix A):

$$\psi_{zz} + (q_e + (1 - q_e)G(\psi_x))\beta^2\psi_{xx} + 2\alpha\beta\phi_{xz} = 0, \quad (26)$$

$$\phi_{zz} + (q_e + (1 - q_e)G(\psi_x))\beta^2\phi_{xx} = 1. \quad (27)$$

The form of this reduced set of equations is very similar to the one in the classical dry scheme proposed in Hoskins and Bretherton (1972), the only difference being the ellipticity coefficient that (in the updraft areas for the MUDD scheme and in the whole domain for the MUMD scheme) is reduced to q_e. As the equivalent potential vorticity is usually much smaller than the potential vorticity, the moist evolution might be expected to be characterized either by smaller horizontal scales or weaker vertical gradients, or a combination of the two. The potential temperature boundary condition, however, still plays a major role in controlling the horizontal scales of the solution to such a boundary-value problem. The relevance of the smallness of the equivalent potential vorticity in contracting the horizontal scales, with respect to the classical dry solution, can be fully understood only after analyzing the solutions derived below.

a. MUMD solution

In the MUMD case G is identically zero and Eqs. (26)–(27) become linear. Assuming as an example that the forcing boundary condition gradient $\theta'_b(x)$ is symmetric, the solution is obtained by means of Fourier sine and cosine transforms:

$$\phi(x, z, t) = \frac{\left(z + \frac{1}{2}\right)^2}{2} + (2/\pi)^{1/2} \times \int_0^\infty \frac{\sinh(\omega h\beta z)\vartheta(\omega)}{\omega h\beta \cosh(\omega h\beta/2)} \times \sin(\omega x)d\omega, \quad (28)$$

$$\psi(x, z, t) = -\alpha\beta(2/\pi)^{1/2}\int_0^\infty \frac{\vartheta(\omega)}{h\beta\cosh(\omega h\beta/2)} \times \left(z\sinh(\omega h\beta z) - \frac{\tanh(\omega h\beta/2)}{2}\cosh(\omega h\beta z)\right) \times \cos(\omega x)d\omega, \quad (29)$$

where

$$\vartheta(\omega) = (2/\pi)^{1/2} \int_0^\infty \theta_b(x) \sin(\omega x) dx. \quad (30)$$

Such a solution is similar to the one of the dry problem (Hoskins and Bretherton 1972), the only difference being the ellipticity coefficient $h\beta$. Frontogenesis is then expected to evolve faster in the moist case as $h = q_e^{1/2}$ approaches 0.

It is also straightforward to verify that

$$\lim_{q_e \to 0} \phi(x, z, t; q_e) = z\theta_b(x) + \frac{\left(z + \frac{1}{2}\right)^2}{2} \quad (31)$$

$$\lim_{q_e \to 0} \psi(x, z, t; q_e) = -\alpha\beta\left(z^2 - \frac{1}{4}\right)\theta_b'(x). \quad (32)$$

Then, in the case of an everywhere cloudy atmosphere that is neutral with respect to conditional slantwise convection, the potential field ϕ remains constant in time, when it is observed in a semigeostrophic coordinate system that is contracting in the horizontal direction at the same rate of the boundary temperature profile. In other words, the rate of frontogenesis, that is, the growth speed of the absolute vorticity, is fully determined by the temperature profile at the surface. The same can be stated about the horizontal and vertical scales of the resulting ageostrophic flow.

As an example, the resulting ageostrophic flow for a forcing temperature profile $\theta_b(x) = 2 \tan^{-1}(x)/\pi$ is plotted in Fig. 1 for the dry case ($q_e = 1$) and in Figs. 2 and 3 for the cases $q_e = 0.1$ and $q_e = 0.01$. The solutions are plotted in a nondimensional physical space $(x', z') = (x - \beta\xi\phi_x, z)$. All the three solutions refer to the time when the maximum absolute vorticity reaches the value $\xi_{max} = 10$. In this way the two solutions may be considered to be at about the same "distance" from the time t_0 of formation of the front. The values of t_0 are 1.20, 0.81, and 0.75 in the first, second, and third cases, respectively. While the maximum updraft velocity increases about three times from the dry

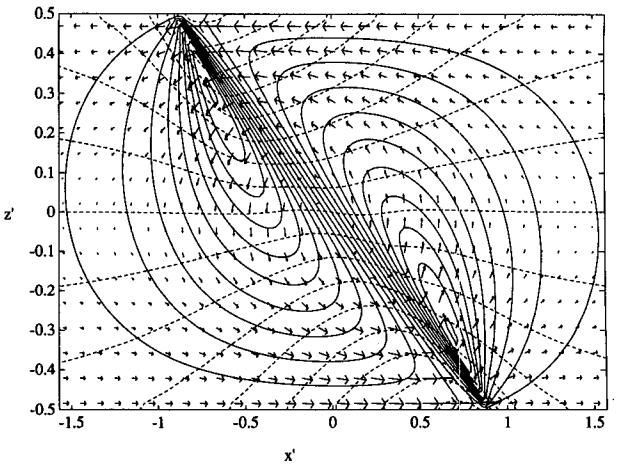

FIG. 2. Ageostrophic flow in nondimensional physical coordinates for $\beta = 2.25$, [$T = 22.5$ h], $q_e = 0.1$, [$Q_e = 4 \times 10^{-8}$ m^2 s^{-1} °K kg^{-1}], $\theta_b(x) = 2 \tan^{-1}(x)/\pi$, [$\Theta_{max} - \Theta_{min} = 20$ K]. Vertical velocity contours (w) are solid, and horizontal velocity contours (u) are dashed. $|w_{max}| = 0.507$, [$|W_{max}| = 0.114$ m s^{-1}]; $|u_{max}| = 1.647$, [$|U_{max}| = 16.47$ m s^{-1}] (MUMD). Dimensional values in square brackets are calculated according to parameter values in Table 1.

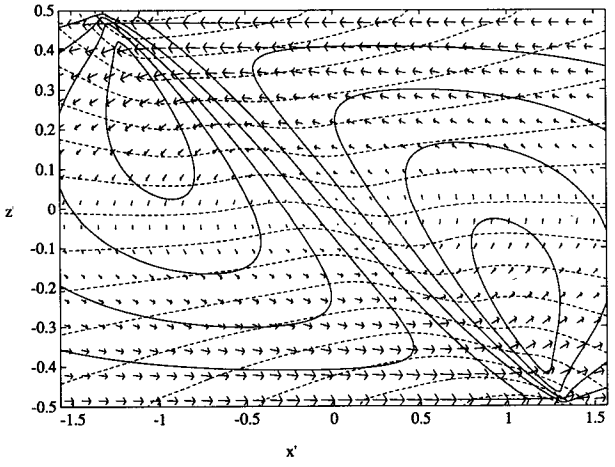

FIG. 1. Ageostrophic flow in nondimensional physical coordinates for $\beta = 3.33$, [$T = 33.4$ h], $q_e = 1.0$, [$Q_e = 4 \times 10^{-7}$ m^2 s^{-1} °K kg^{-1}], $\theta_b(x) = 2 \tan^{-1}(x)/\pi$, [$\Theta_{max} - \Theta_{min} = 20$ K]. Vertical velocity contours (w) are solid, and horizontal velocity contours (u) are dashed. $|w_{max}| = 0.227$, [$|W_{max}| = 0.076$ m s^{-1}]; $|u_{max}| = 1.680$, [$|U_{max}| = 16.80$ m s^{-1}] (MUMD). Dimensional values in square brackets are calculated according to parameter values in Table 1.

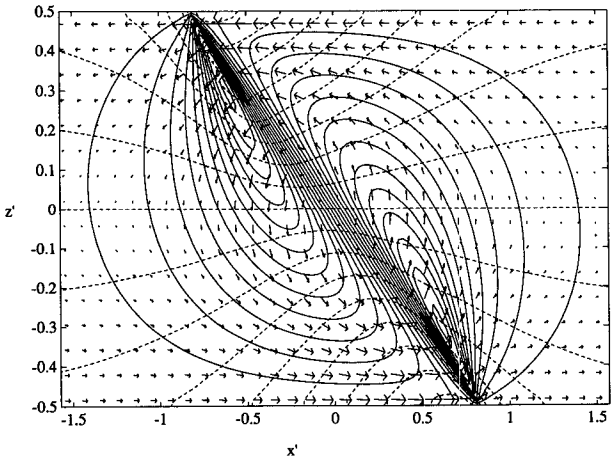

FIG. 3. Ageostrophic flow in nondimensional physical coordinates for $\beta = 2.11$, [$T = 20.7$ h], $q_e = 0.01$, [$Q_e = 4 \times 10^{-9}$ m^2 s^{-1} °K kg^{-1}], $\theta_b(x) = 2 \tan^{-1}(x)/\pi$, [$\Theta_{max} - \Theta_{min} = 20$ K]. Vertical velocity contours (w) are solid, and horizontal velocity contours (u) are dashed. $|w_{max}| = 0.618$, [$|W_{max}| = 0.131$ m s^{-1}]; $|u_{max}| = 1.666$, [$|U_{max}| = 16.66$ m s^{-1}] (MUMD). Dimensional values in square brackets are calculated according to parameter values in Table 1.

case to the moist case with $q_e = 0.01$, the maximum horizontal ageostrophic velocity remains about the same. The increasing maximum updraft velocity corresponds to decreasing characteristic horizontal scales, which tend to be narrower for smaller equivalent potential vorticities. There is however, no singular behavior as q_e goes to 0, as also shown by the limits (31) and (32). In particular, the horizontal scales of the vertical velocity are bounded from below by the horizontal scales of the function $\theta_b''(x)/(1 - \beta^2 z\theta_b''(x))$. This tendency is evident in the Figs. 1, 2 and 3, where the differences between the cases $q_e = 1$ and $q_e = 0.1$, both in terms of magnitude and scales of the vertical velocity, are much bigger than the ones between the cases $q_e = 0.1$ and $q_e = 0.01$.

The magnitude of the horizontal ageostrophic velocity and its time evolution are crucial for the validation of the semigeostrophic scheme [see (22)]. It turns out that the MUMD scheme satisfies the semigeostrophic assumptions also for vanishing equivalent potential vorticity q_e. As an illustration, Figs. 4, 5, and 6 show the time evolution of vorticity, horizontal, and vertical ageostrophic velocities, for values of q_e in the range [0, 1]. We observe from the maximum absolute vorticity graph (Fig. 4) that the frontogenesis evolution becomes faster and faster as the equivalent potential vorticity decreases, but with no singular behavior as that parameter vanishes. Each curve tends to a vertical asymptote located at the time t_0 of the formation of the front. The evolution of the maximum values of the corresponding ageostrophic horizontal and vertical velocities is shown in Figs. 5 and 6, respectively, up to the time when $\xi_{\max} > 10$ for each particular value of equivalent potential vorticity. Only the vertical velocity is sensitive, in its maximum values, to the variations of the equivalent potential vorticity. Close to the time of the front formation, the maximum vertical velocity

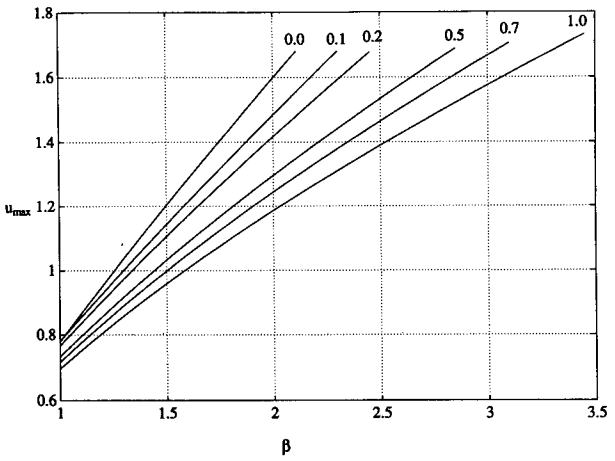

FIG. 5. Evolution of the maximum ageostrophic horizontal velocity, for $\theta_b(x) = 2\tan^{-1}(x)/\pi$ and various values of q_e (labels on top of graphs), as a function of the time parameter $\beta = \exp(t)$ (MUMD).

in the conditionally neutral atmosphere ($q_e = 0$) is almost four times larger than the one in the dry case ($q_e = 1$).

Because the MUMD solutions are "well behaved" in the whole range $q_e \in [0, 1]$, it is of some interest to study the behavior of the same problem for negative values of the equivalent potential vorticities. As mentioned in the Introduction, an analytical study of conditional symmetric instabilities in the presence of frontogenesis requires the formulation, in analytical form, of the undisturbed base circulation for $q_e < 0$. In this case Eqs. (26) and (27) are hyperbolic, but the reduced problem is still linear given that $G = 0$ in the MUMD scheme. Provided then that the boundary conditions are not given along the characteristic lines (whose slopes are $\pm q_e^{1/2}$), the solution is still unique,

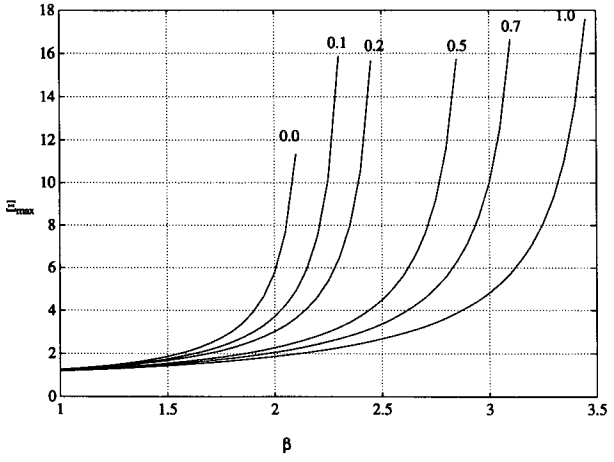

FIG. 4. Evolution of the maximum absolute vorticity, for $\theta_b(x) = 2\tan^{-1}(x)/\pi$ and various values of q_e (labels on top of graphs), as a function of the time parameter $\beta = \exp(t)$: (MUMD).

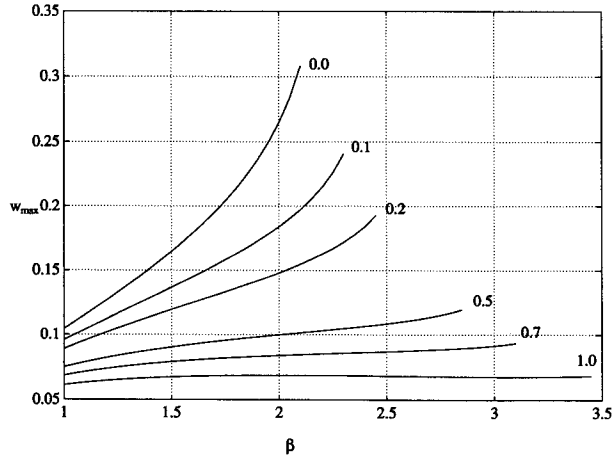

FIG. 6. Evolution of the maximum vertical velocity, for $\theta_b(x) = 2\tan^{-1}(x)/\pi$ and various values of q_e (labels on top of graphs), as a function of the time parameter $\beta = \exp(t)$: (MUMD).

and it can be simply obtained by replacing ih (i = imaginary unit) for h in (28) and (29). The integration of the solution Fourier transform, however, is now more problematic. A simpler case results by replacing the lateral conditions for $x \to \pm\infty$ by periodicity conditions. A simple sinusoidal profile is assumed for the boundary potential temperature. It is generally supposed that the semigeostrophic approximation breaks down when $q_e < 0$. This does not occur in the MUMD scheme, however, when q_e is uniform: the geostrophic momentum approximation along the cross-front direction is still valid in a range of forcing conditions and time. While it is well known that such a solution will be unstable to small perturbations, there is nothing to prevent the solution from being obtained, if for no other reason than to provide a slowly evolving base state on which to examine the growth of unstable perturbations. As shown in appendix C, even semigeostrophic perturbations to such solutions can be unstable. The time evolution of the maxima of the absolute vorticity and of the ageostrophic velocities are plotted in Figs. 7, 8, and 9 for $q_e \in [-1, 1]$. These plots are equivalent to Figs. 4, 5, and 6, which corresponded to an arctangent potential temperature profile and were limited to $q_e \in [0, 1]$. Two different sinusoidal forcing profiles with amplitude 0.3 (solid lines) and 0.6 (dashed lines) and unitary wavelength have been assumed in the examples shown. From a qualitative point of view, the only relevant difference with respect to Figs. 4, 5, and 6 is in the behavior of the horizontal velocity. It is now much more sensitive to the variations in the equivalent potential vorticity. This can be explained observing the functional dependence of the periodic solutions on $h = q_e^{1/2}$: the horizontal scales remain fully controlled by the boundary condition wavelength, and only the vertical scales are affected by the decreasing equivalent potential vorticity. The maximum horizontal velocity occurs on the horizontal boundaries, where the vertical one is null, so it depends only on the vertical derivative of the ageostrophic streamfunction ($u(z = \pm 1/2) = \psi_z$). The temporal growth of the horizontal velocity, however, is still much slower than that of the other variables, and the rate of growth becomes negative prior to the formation of the front for certain ranges of equivalent potential vorticity. The vertical velocity monotonically increases as the equivalent potential vorticity decreases from positive values. The horizontal velocity, on the other hand, achieves a maximum value for $q_e = 0$.

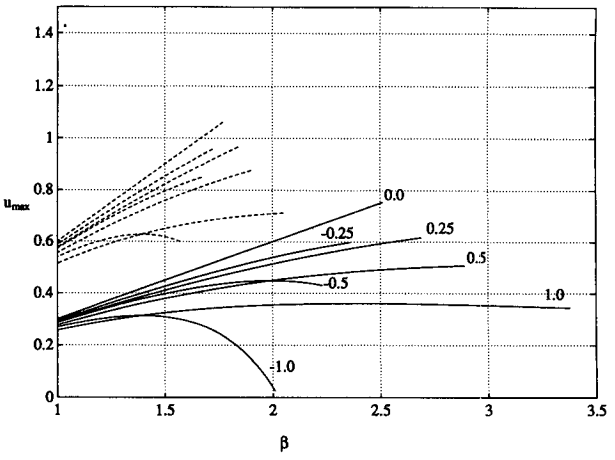

FIG. 8. Evolution of the maximum ageostrophic horizontal velocity, for $\theta_b(x) = 0.3 \sin(x)$ (solid lines) and $f(x) = 0.6 \sin(x)$ (dashed lines) and various values of q_e (labels on top of graphs), as a function of the time parameter $\beta = \exp(t)$: (MUMD).

b. *MUDD solution*

The next step is to study the nonlinear behavior of the moist frontogenesis dynamics when no evaporation

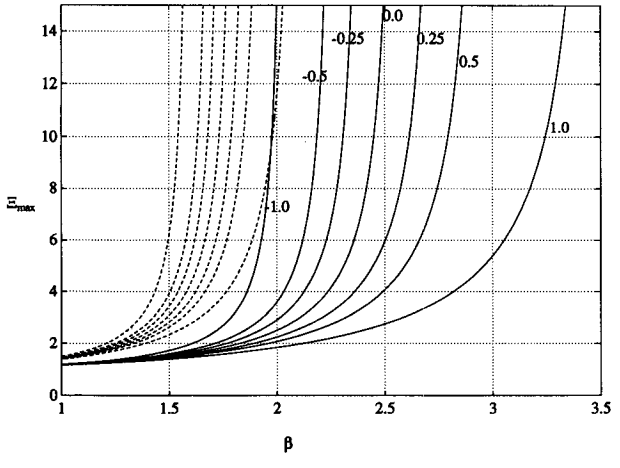

FIG. 7. Evolution of the maximum absolute vorticity, for $f(x) = 0.3 \sin(x)$ (solid lines) and $\theta_b(x) = 0.6 \sin(x)$ (dashed lines) and various values of q_e (labels on top of graphs), as a function of the time parameter $\beta = \exp(t)$: (MUMD).

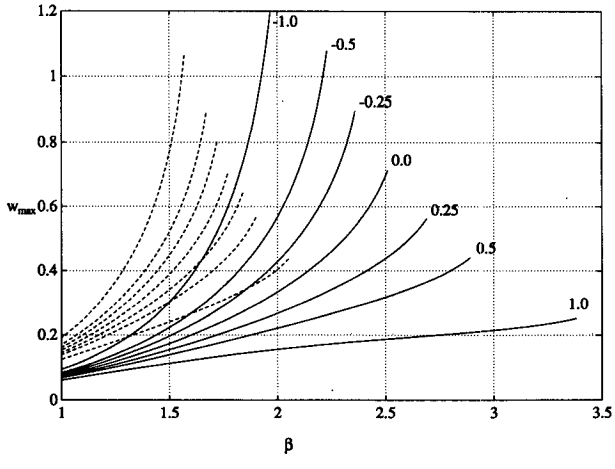

FIG. 9. Evolution of the maximum vertical velocity, for $\theta_b(x) = 0.3 \sin(x)$ (solid lines) and $f(x) = 0.6 \sin(x)$ (dashed lines) and various values of q_e (labels on top of graphs), as a function of the time parameter $\beta = \exp(t)$: (MUMD).

is presumed in the downdraft. This is the more realistic MUDD scheme.

The new set of Eqs. (26)–(27) remains nonlinear in the MUDD case, where the parameter G is a function of one of the dependent variables. The proposed solutions involve the assumption that the whole domain can be subdivided in one updraft and one downdraft area (Emanuel 1985), separated by an interface that remains nearly vertical, in semigeostrophic coordinates, at any time, even if moving in space. Equations (26)–(27) can be then separated and a particular solution obtained (appendix B).

Such a particular solution may be thought as a combination of the "dry" and the MUMD ones, plus additional terms that need to be introduced to maintain the continuity of the various velocity and potential temperature fields at the interface position $x = l$. Such additional terms become singular in the limits ($q_e \to 0$; $x \to l$); a singular perturbation method needs then to be used to study the MUDD solution for vanishing equivalent potential vorticity near the separation interface. Only the case of finite positive values of q_e will be addressed here.

As an example of the solutions for the MUDD scheme, the resulting ageostrophic flows for the same forcing temperature profile adopted in the examples of the MUDD solution, for $q_e = 0.25$ and $q_e = 0.1$ at the times when $\xi_{max} = 10$, are shown in Figs. 10 and 11. Comparing the timing of the front formation in the second one with the analogous MUMD case, we observe how the frontogenesis process is slightly retarded by the presence of dry evolution in the downdraft area. Because of this damping effect the updraft velocity is less intense than the one in the analogous MUMD case. We can also observe that the asymmetric thermodynamical behavior is reflected in the loss of symmetry of the ageostrophic flow, mainly in its vertical component. The updraft velocity is found to be much more intense and more concentrated near the front than the downdraft velocity. This is due to the scale contraction in the streamfunction field and to the faster growth of the absolute vorticity in the area with moist evolution. Also, the front will tend to develop first at the ground and later at the tropopause.

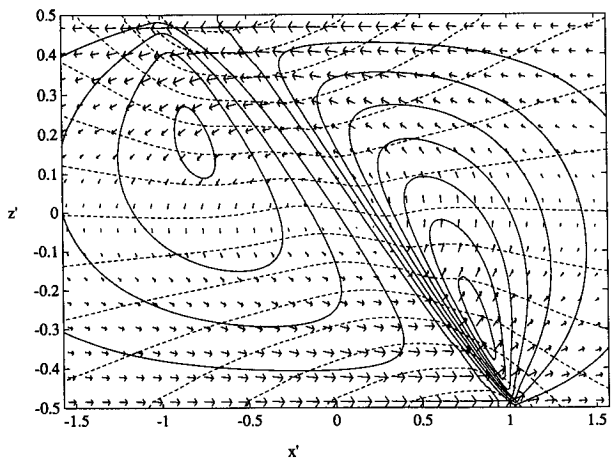

FIG. 10. Ageostrophic flow in nondimensional physical coordinates for $\beta = 2.60$, [$T = 26.5$ h], $q_e = 0.25$, [$Q_e = 10^7$ m^2 s^{-1} °K kg^{-1}], $\theta_b(x) = 2\tan^{-1}(x)/\pi$, [$\Theta_{max} - \Theta_{min} = 20$ K]. Vertical velocity contours (w) are solid, and horizontal velocity contours (u) are dashed. $w_{max} = 0.370$, [$W_{max} = 0.096$ m s^{-1}]; $w_{min} = -0.206$, [$W_{min} = -0.054$ m s^{-1}]; $|u_{max}| = 1.666$, [$|U_{max}| = 16.66$ m s^{-1}] (MUDD). Dimensional values in square brackets are calculated according to parameter values in Table 1.

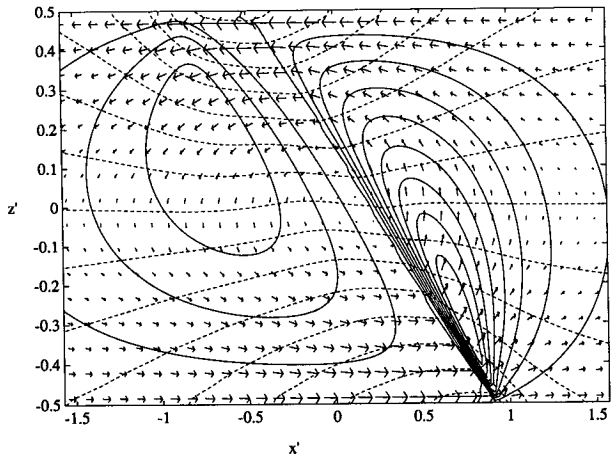

FIG. 11. Ageostrophic flow in nondimensional physical coordinates for $\beta = 2.24$, [$T = 22.4$ h], $q_e = 0.1$, [$Q_e = 4 \times 10^{-8}$ m^2 s^{-1} °K kg^{-1}], $\theta_b(x) = 2\tan^{-1}(x)/\pi$, [$\Theta_{max} - \Theta_{min} = 20$ K]. Vertical velocity contours (w) are solid, and horizontal velocity contours (u) are dashed. $w_{max} = 0.444$, [$W_{max} = 0.099$ m s^{-1}]; $w_{min} = -0.190$, [$W_{min} = -0.043$ m s^{-1}]; $|u_{max}| = 1.461$, [$|U_{max}| = 14.61$ m s^{-1}] (MUDD). Dimensional values in square brackets are calculated according to parameter values in Table 1.

A clearer idea about the quantitative difference between the MUMD and MUDD solutions can be obtained by referring again to the temporal evolution of the maxima of the absolute vorticity and of the ageostrophic velocities, given the same arctangent boundary temperature profile and display criteria previously adopted (Figs. 12, 13, and 14). The time evolution of the maximum value of the vertical component of the absolute vorticity (Fig. 12), which is indicative of the degree of frontogenesis reached by the system, seems to be somewhat slower in the MUDD cases, but only for finite values of the equivalent potential vorticity. On the other hand, when the equivalent potential vorticity is very small the evolution of the front in the MUDD cases is much faster, with a clear tendency toward a singular "instantaneous" frontogenesis. No significant difference is evident, among the two schemes, in the maximum values of the horizontal ageostrophic velocity (Fig. 13). They maintain about the same value if the frontogenesis evolution is at the same stage. Significant differences are nevertheless present in the evolution of the extreme values of the

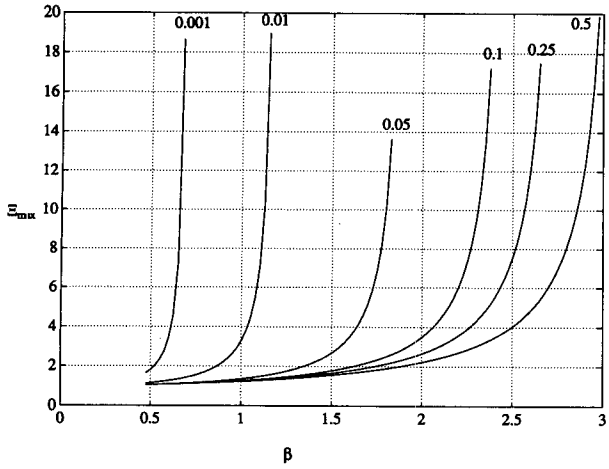

FIG. 12. Evolution of the maximum absolute vorticity, for $\theta_b(x) = 2\tan^{-1}(x)/\pi$ and various values of q_e (labels on top of graphs), as a function of the time parameter $\beta = \exp(t)$: (MUDD).

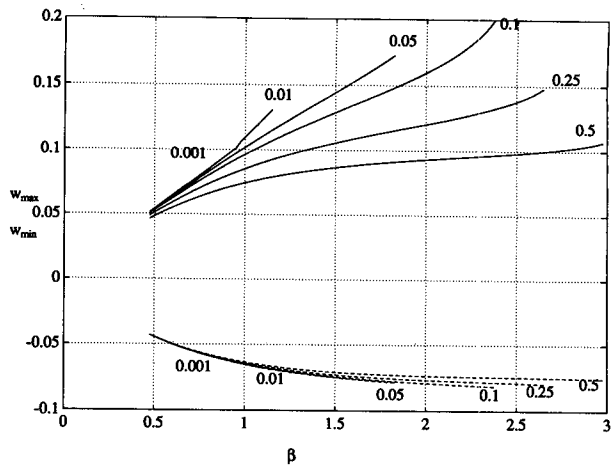

FIG. 14. Evolution of the maximum (solid lines) and minimum (dashed lines) vertical velocity, for $\theta_b(x) = 2\tan^{-1}(x)/\pi$ and various values of q_e (labels on top of graphs), as a function of the time parameter $\beta = \exp(t)$: (MUDD).

vertical velocity (Fig. 14, where the minima are also plotted). For equivalent potential vorticities between 0.1 and 0.5 the maximum updraft velocity is of the same order of magnitude as that in the MUMD case, although slightly smaller. The minimum downdraft velocity is not very sensitive to the particular value of q_e and remains very similar to that of the dry case. But when $q_e \ll 0.1$ the fast growth of the absolute vorticity does not allow for full development of the ageostrophic flow, and the velocities are still relatively small at the time of the front formation.

Two different and important approximations were made to arrive at the proposed particular MUDD solution. First was the assumption that the interface between updraft and downdraft areas, in semigeostrophic space, remains vertical. Second was neglecting the potential vorticity variations in the downdraft area, caused by the progressive translation of the separation interface.

The first assumption is found to be almost exact. The vertical velocity, calculated at the position $x = l$, is, for all the many different cases, an order of magnitude smaller than the overall accuracy of the calculation of the solution. Figure 15 shows the resulting ageostrophic flow in semigeostrophic coordinates for $q_e = 0.01$ when $\xi_{max} = 10$, where the vertical position of the separation boundary is evident.

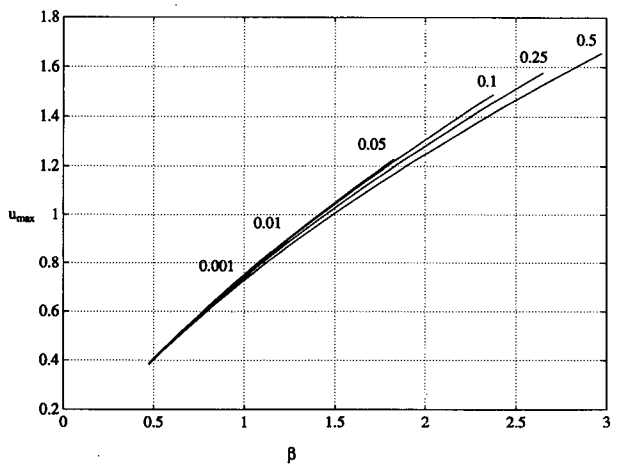

FIG. 13. Evolution of the maximum ageostrophic horizontal velocity, for $\theta_b(x) = 2\tan^{-1}(x)/\pi$ and various values of q_e (labels on top of graphs), as a function of the time parameter $\beta = \exp(t)$: (MUDD).

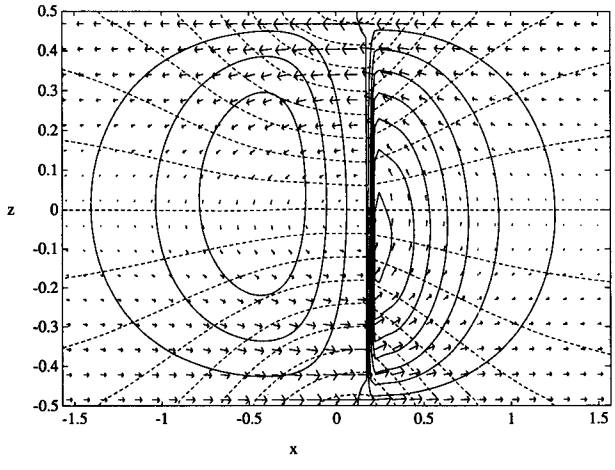

FIG. 15. Ageostrophic flow in nondimensional semigeostrophic coordinates for $\beta = 1.16$, [$T = 4.12$ h], $q_e = 0.01$, [$Q_e = 4 \times 10^{-9}$ m^2 s^{-1} °K kg^{-1}], $\theta_b(x) = 2\tan^{-1}(x)/\pi$, [$\Theta_{max} - \Theta_{min} = 20$ K]. Vertical velocity contours (w) are solid, and horizontal velocity contours (u) are dashed. $w_{max} = 0.149$, [$W_{max} = 0.017$ m s^{-1}]; $w_{min} = -0.080$, [$W_{min} = -0.009$ m s^{-1}]; $|u_{max}| = 0.838$, [$|U_{max}| = 8.380$ m s^{-1}] (MUDD). Dimensional values in square brackets are calculated according to parameter values in Table 1.

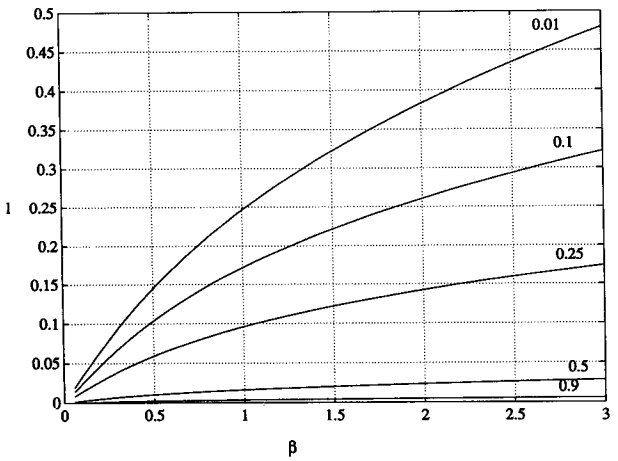

FIG. 16. Horizontal displacement, with respect to the center of the domain, of the vertical separation boundary $l(\beta = \exp(t))$, for $\theta_b(x) = 2\tan^{-1}(x)/\pi$ and various values of q_e (labels on top of graphs).

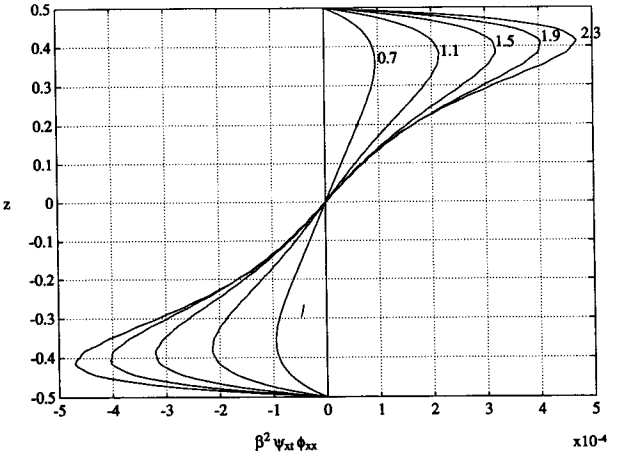

FIG. 18. Vertical profile of the neglected term $\beta^2\psi_{xl}\phi_{xx}$, calculated at the separation boundary $x = l(t)$, for $\theta_b(x) = 2\tan^{-1}(x)/\pi$, $q_e = 0.1$ and various values of β (labels near the graphs).

The progressive translation of the separation interface between updraft and downdraft areas is by itself not negligible, as shown in Fig. 16. Its position $x = l(t)$ is depicted, calculated as described in appendix B, for various values of the equivalent potential vorticity. When q_e approaches 0, the magnitude of the boundary translation velocity is almost of order of magnitude one. However, its effect on the potential vorticity evolution can be measured by the term $\beta^2\psi_{xl}\phi_{xx}$ evaluated at $x = l$ [Eq. (A.9)]. Figures 17 and 18 show the values of that term calculated at various times for $q_e = 0.25$ and $q_e = 0.1$ and the same arctangent forcing temperature profile used in the previous examples. These values are to be compared with the magnitude of the other terms in the assumed equations, which are of order of magnitude one. We may then conclude that this approximation is of the same order as, or even smaller than, that of the semigeostrophic approximation itself. This may be explained considering that, even if the translation velocity of the separation boundary is not small, it is toward the warm (updraft) side. On the cold (downdraft) side, in proximity of the boundary, the vertical velocity is very small, such that the consequent "dry" evolution of the potential vorticity is very slow.

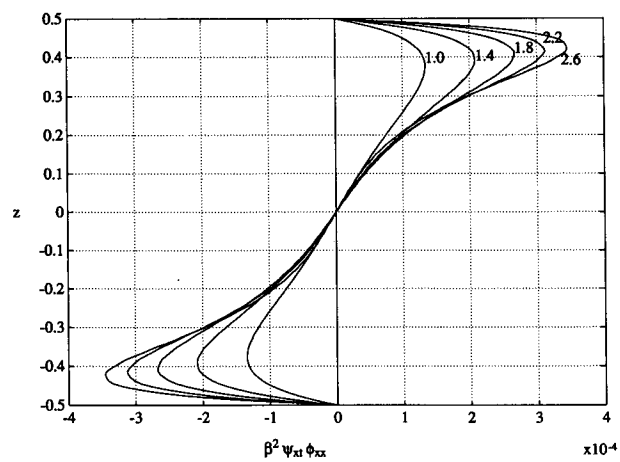

FIG. 17. Vertical profile of the neglected term $\beta^2\psi_{xl}\phi_{xx}$, calculated at the separation boundary $x = l(t)$, for $\theta_b(x) = 2\tan^{-1}(x)/\pi$, $q_e = 0.25$ and various values of β (labels near the graphs).

4. Conclusions

A semigeostrophic model of moist frontogenesis has been briefly reviewed in order to investigate the possibility of obtaining analytical solutions to the resulting nonlinear problem. Such a task is needed in, among other things, the study of the interaction between frontal circulations and mesoscale instabilities, when frontogenesis takes place in an environment that is unstable with respect to moist slantwise convection.

A method for obtaining a particular solution has been proposed, based on the inversion of the geopotential equation and on the dependence between the resulting potential vorticity equation and the streamfunction equation.

In the case where condensation is retained as the only diabatic process in a saturated atmosphere, this approach leads to the formulation of separate linear problems inside each region where the vertical velocity does not change sign.

If a cloudy atmosphere is assumed and evaporation is considered (MUMD), a reduced linear problem, similar to the dry one, is obtained and solved using Fourier transforms. The use of this first simplified scheme leads to a better understanding of the basic effects of the diabatic heat exchanges on the resulting ageostrophic flow. Such effects include a faster contraction in both the temporal scales of the frontogenesis

and the horizontal spatial scales of the vertical velocity. The obtained particular solution is shown to be valid also for negative equivalent potential vorticity. In this last case, the growth of symmetric instabilities is expected, ultimately leading to a breakdown in the validity of the semigeostrophic approximation. Furthermore, the cross-front horizontal velocity becomes weaker for negative equivalent potential vorticity, slowing down prior to the front formation. Further investigations are needed to understand the physical relevance of such behavior.

The reduced problem is still nonlinear in the case where only condensation is considered (MUDD). The position of the separation boundary between updraft and downdraft areas is a function of the resulting ageostrophic flow. An approximate particular solution is obtained. This solution is based on the assumptions that the separation boundary is a vertical interface in semigeostrophic coordinates, and that the effect of the moving interface on the dynamics is small. Both assumptions are verified a posteriori. The introduction of an asymmetric scheme for the diabatic heating leads to two main differences in the derived solutions relative to the symmetric MUMD case. Namely, large differences are found among the characteristic scales and intensities of the updraft and downdraft velocities, and singular behavior of the frontogenetic process is observed in the limit $q_e \to 0$.

The MUMD solution may be considered as a valid unperturbed zero-order solution of the frontal circulation in a moist unstable atmosphere, where evaporation is also relevant. Higher-order approximations to the frontal circulation, including ageostrophic accelerations, may be then obtained and used to study the growth of moist symmetric instabilities in a forcing environment. Further investigations are needed to fully assess the properties of the MUDD solutions for vanishing and negative values of the equivalent potential vorticity.

Acknowledgments. The support of the National Research Council of Italy, through a cooperative agreement between the University of Florence and M.I.T., is acknowledged and very much appreciated. We also acknowledge the support of the National Science Foundation, with a project on the Predictability of Mesoscale Precipitation (ATM-9020832).

APPENDIX A

A Method for Obtaining a Particular Solution to the Set of Eqs. (22)–(23)

In this appendix a method for obtaining a particular solution to the nonlinear set of Eqs. (24)–(25) with uniform initial conditions for the potential vorticity is discussed. The method is based on the reduction of the original set of equations to a simpler system.

Suppose that the following equalities hold:

$$(\beta^2\phi_x)_t = -\beta\psi_z, \tag{A1}$$

$$\phi_{zt} = (q_e + (1 - q_e)G(\psi_x))\beta\psi_x. \tag{A2}$$

Cross deriving and subtracting leads to

$$\psi_{zz} + (q_e + (1 - q_e)G(\psi_x))\beta^2\psi_{xx} + 2\alpha\beta\phi_{xz} = 0, \tag{A3}$$

where it is assumed that ($\delta(\cdot)$ being the Dirac function):

$$\delta(\psi_x)\psi_x \approx 0. \tag{A4}$$

Hence, given the homogeneous lateral conditions for all the horizontal gradients and the homogeneous conditions for ϕ_{zt} and ψ on the top and bottom boundaries, relations (A1) and (A2) are proven to satisfy the streamfunction equation (25).

Inverting the order of derivation, the following equation for the geopotential is obtained:

$$\phi_{zzt} + (q_e + (1 - q_e)G(\psi_x))(\beta^2\phi_{xx})_t = 0. \tag{A5}$$

After integration by parts with respect to time, this is transformed to

$$\phi_{zz} + (q_e + (1 - q_e)G(\psi_x))\beta^2\phi_{xx} = \int \beta^2 G'(\psi_x)\psi_{xt}\phi_{xx}dt + \text{const.} \tag{A6}$$

Substitution of relations (A1) and (A2) in the geopotential equation (24) leads to the following equation:

$$\{(1 - \beta^2\phi_{xx})\beta\psi_{xz}(1 - \beta^2\phi_{xx} - \phi_{zz}) - \beta\psi_x(\phi_{zzz}(1 - \beta^2\phi_{xx}) + \beta^2\phi_{zz}\phi_{xxz})\} \times G(\psi_x) = 0. \tag{A7}$$

Such an equation is identically satisfied in the MUMD case ($G = 0$). In the MUDD case it is satisfied only in an approximate manner, neglecting the effect of the time dependence of the position of the interface between updraft and downdraft areas. Equation (A5) is then integrated with respect to time, given the initial condition for the potential vorticity, to obtain

$$\phi_{zz} + (q_e + (1 - q_e)G(\psi_x))\beta^2\phi_{xx} = 1. \tag{A8}$$

This approximation corresponds to the assumption (letting $G'(\cdot) = \delta(\cdot)$):

$$\int \beta^2\delta(\psi_x)\psi_{xt}\phi_{xx}dt = 0. \tag{A9}$$

APPENDIX B

Approximate Solution to the MUDD Scheme

Consider the following system of partial differential equations:

$$\phi_{zz} + a^2\phi_{xx} = 1, \tag{B1}$$

$$\psi_{zz} + a^2\psi_{xx} + 2\alpha\beta\phi_{xz} = 0 \quad \text{(B2)}$$

with boundary conditions (16)–(20). In such a problem, time appears only as a coefficient, and will not be considered here as an explicit independent variable. Given a smooth boundary thermal profile with unimodal horizontal gradient (for example, the arctangent function), we look for a solution such that the whole spatial domain can be subdivided in two areas inside of which the sign of the vertical velocity remains constant (one updraft and one downdraft):

$$a^2 = \beta^2(1 - (1 - q_e)H(x - 1)). \quad \text{(B3)}$$

In general, it will be $l = l(x)$, so that the above system of equations is not separable. We then make the approximation l = const. (in space), such that we may write

$$\phi = z\theta_b(x) + \frac{\left(z + \frac{1}{2}\right)^2}{2} + \sum_n^\infty \phi_n(x)\sin(n\pi z), \quad \text{(B4)}$$

$$\psi = \sum_n^\infty \psi_n(x)\cos(n\pi z), \quad \text{(B5)}$$

and the following infinite set of coupled ordinary differential equations for the unknown Fourier coefficients is obtained:

$$\left.\begin{aligned} a^2\phi_n'' - n^2\pi^2\phi_n + a^2 Z_n\theta_b'' = 0 \\ a^2\psi_n'' - n^2\pi^2\psi_n + 2\alpha\beta n\pi\phi_n + 2\alpha\beta n\pi Z_n\theta_b'' = 0 \end{aligned}\right\}, \quad n = 1, 3, 5, \cdots, \infty, \quad \text{(B6)}$$

where $Z = [4(-1)^{(n-1)/2}]/(n^2\pi^2)$, $n = 1, 3, 5, \cdots, \infty$. Let (for a symmetric temperature profile)

$$\vartheta(\omega) = (2/\pi)^{1/2}\int_0^\infty \theta_b'(x)\cos(\omega x)dx. \quad \text{(B7)}$$

Then the general solution to the set of ordinary differential equations (B6) can be written as

$$\phi_n = -(2/\pi)^{1/2}\int_0^\infty \frac{\omega a^2 Z_n\vartheta(\omega)}{\omega^2 a^2 + n^2\pi^2}\sin(\omega x)d\omega + B_n\exp\left(\frac{n\pi}{a}|x - 1|\right), \quad \text{(B8)}$$

$$\psi_n = \alpha\beta n(2/\pi)^{1/2}\int_0^\infty \frac{n^2\pi^2 Z_n\vartheta(\omega)}{(\omega^2 a^2 + n^2\pi^2)^2}\cos(\omega x)d\omega + \left(C_n - \frac{\alpha\beta n\pi B_n}{a^2}(x - 1)\right)\times\exp\left(\frac{n\pi}{a}|x - 1|\right), \quad \text{(B9)}$$

where

$$B_n = B_n^- - (B_n^- - B_n^+)H(x - 1), \quad \text{(B10)}$$

$$C_n = C_n^- - (C_n^- - C_n^+)H(x - 1). \quad \text{(B11)}$$

The sets of coefficients $\{B_n^+, B_n^-, C_n^+, C_n^-\}$ is determined by requiring continuity of the velocity and temperature fields; that is, ϕ, ϕ_x, ψ, ψ_x, at $x = l$. The following results are then obtained:

$$B_n^- = (2/\pi)^{1/2}\int_0^\infty \frac{(1 - q_e^{1/2})\omega\beta^2 n\pi Z_n\vartheta(\omega)}{(\omega^2\beta^2 q_e + n^2\pi^2)(\omega^2\beta^2 + n^2\pi^2)} \times (q_e^{1/2}\beta\omega\cos(\omega l) + n\pi\sin(\omega l))d\omega, \quad \text{(B12)}$$

$$B_n^+ = (2/\pi)^{1/2}\int_0^\infty \frac{(1 - q_e^{1/2})\omega\beta^2 n\pi Z_n\vartheta(\omega)}{(\omega^2\beta^2 q_e + n^2\pi^2)(\omega^2\beta^2 + n^2\pi^2)} \times (q_e^{1/2}\beta\omega\cos(\omega l) - q_e^{1/2}n\pi\sin(\omega l)d\omega, \quad \text{(B13)}$$

$$C_n^- = 2\alpha\beta^2(2/\pi)^{1/2}\int_0^\infty \frac{\omega n^2\pi^2 Z_n\vartheta(\omega)}{(\omega^2\beta^2 + n^2\pi^2)^2} \times \sin(\omega l)d\omega + \alpha B_n^-, \quad \text{(B14)}$$

$$C_n^+ = -2\alpha\beta^2 q_e^{1/2}(2/\pi)^{1/2}\int_0^\infty \frac{\omega n^2\pi^2 Z_n\vartheta(\omega)}{(\omega^2\beta^2 q_e + n^2\pi^2)^2} \times \sin(\omega l)d\omega - \frac{\alpha B_n^+}{q_e^{1/2}}. \quad \text{(B15)}$$

The position l of the separation interface between updraft and downdraft areas, according to the previously introduced approximation, is found by setting $\psi_{1,x}(x = l) = 0$, that is, by approximating the vertical velocity by its first Fourier coefficient only. This leads to the condition:

$$\int_0^\infty \frac{G(\omega)\vartheta(\omega)}{(\omega^2\beta^2 q_e + n^2\pi^2)^2(\omega^2\beta^2 + n^2\pi^2)^2}d\omega = 0, \quad \text{(B16)}$$

where

$$G(\omega) = \{2\pi^2((\omega^2\beta^2 q_e + \pi^2)^2 - (\omega^2\beta^2 + \pi^2)^2) + (1 - q_e)\omega^2\beta^2(\omega^2\beta^2 q_e + \pi^2)(\omega^2\beta^2 + \pi^2)\} \times \cos(\omega l) + 2\pi\beta\omega\{(\omega^2\beta^2 q_e + \pi^2)^2 + q_e^{1/2}(\omega^2\beta^2 + \pi^2)^2\}\sin(\omega l). \quad \text{(B17)}$$

The calculation of the vertical velocity at such a boundary using a less crude truncation of the Fourier series will serve as an "a posteriori" verification on the error introduced with the vertical separation boundary approximation.

APPENDIX C

Linear Stability of the MUMD Solution to Semigeostrophic Perturbations

Given that the MUDD solutions have been discussed for positive values of the equivalent potential vorticity

only, when the system of equations was strictly of an elliptic type, the stability analysis of the proposed particular solutions will be confined to the case of the MUMD scheme.

For the sake of simplicity, we then consider the solution (ϕ^*, ψ^*) to the case with periodic lateral conditions, to which we add some infinitesimal perturbations $(\delta\phi, \delta\psi)$ that satisfy the homogeneous boundary conditions. The perturbed solutions are then:

$$\phi(x, z, t) = \phi^*(x, z, t) + \delta\phi(x, z, t) = \left\{ \frac{\left(z + \frac{1}{2}\right)^2}{2} + \theta_b \frac{\sinh(kh\beta z)}{kh\beta \cosh(kh\beta/2)} \sin(kx) \right\} + P(t) \sin(mkx) \sin(n\pi z), \quad \text{(C1)}$$

$$\psi(x, z, t) = \psi^*(x, z, t) + \delta\psi(x, z, t) = -\left\{ \frac{\alpha\beta^2\theta_b}{h\beta \cosh(kh\beta/2)} \left(z \sinh(kh\beta z) - \frac{\tanh(kh\beta/2)}{2} \cosh(kh\beta z) \right) \cos(kx) \right\} + Y(t) \cos(mkx) \cos(n\pi z), \quad \text{(C2)}$$

where k is the wavelength of the potential temperature forcing profile and the amplitude P of the geopotential perturbation is supposed to be infinitesimal at some arbitrary initial time t_0 ($P_0 \ll 1$). The streamfunction perturbation, of amplitude Y, is supposed to be balanced by the geopotential perturbation. The undisturbed solution (ϕ^*, ψ^*) is simply obtained assuming in expressions (28) and (29) a single-frequency spectrum for the forcing temperature profile.

The substitution of the perturbed solutions in equations (24) and (25), with $G = 0$, leads to the following set of equations:

$$\{\phi^*_{zzt} + \delta\phi_{zzt} - q_e\beta\psi^*_{xz} - q_e\beta\delta\psi_{xz}\} \times (1 - \beta^2\phi^*_{xx} - \beta^2\delta\phi_{xx}) + (\phi^*_{zz} + \delta\phi_{zz}) \times \{(\beta^2\phi^*_{xx})_t + (\beta^2\delta\phi_{xx})_t + \beta\psi^*_{xz} + \beta\delta\psi_{xz}\} = 0, \quad \text{(C3)}$$

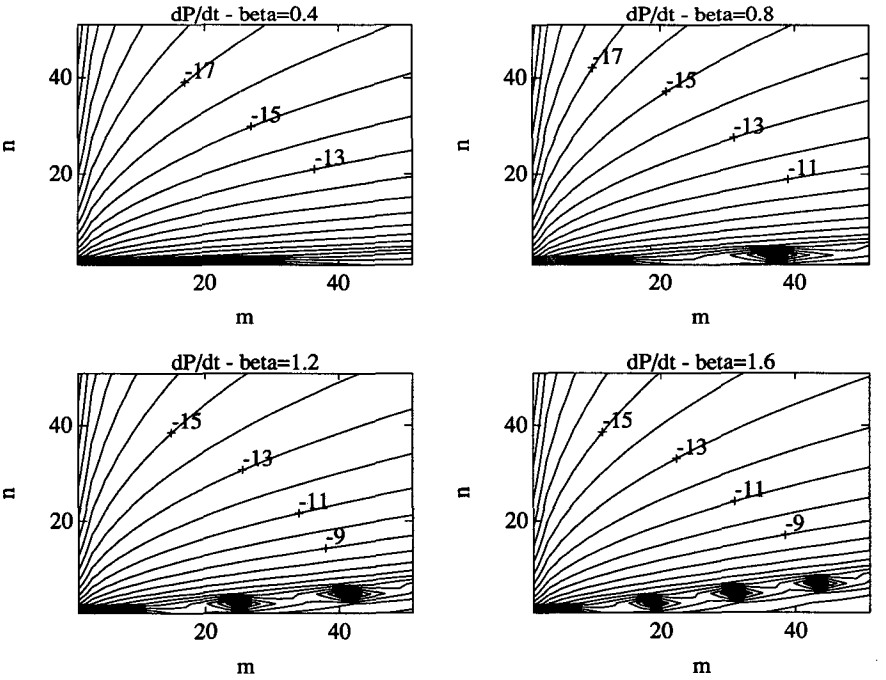

FIG. A1. Contours of the growth rate (in logarithmic scale) of periodic infinitesimal potential perturbations in a conditionally unstable atmosphere ($q_e = -0.1$), as a function of the wave numbers in the horizontal (m) and vertical (n) directions.

$$\psi^*_{zz} + \delta\psi_{zz} + q_e\beta^2\psi^*_{xx} + q_e\beta^2\delta\psi_{xx} + 2\alpha\beta\phi^*_{xz} + 2\alpha\beta\delta\phi_{xz} = 0, \quad \text{(C4)}$$

which, by using relations (A1) and (A2) and Eq. (24), and after linearization with respect to the perturbations, simplifies to

$$\{\delta\phi_{zzt} - q_e\beta\delta\psi_{xz}\}(1 - \beta^2\phi^*_{xx}) + \phi^*_{zz}\{(\beta^2\delta\phi_{xx})_t + \beta\delta\psi_{xz}\} = 0, \quad \text{(C5)}$$

$$\delta\psi_{zz} + q_e\beta^2\delta\psi_{xx} + 2\alpha\beta\delta\phi_{xz} = 0. \quad \text{(C6)}$$

Given the periodic form of the perturbations, the second equation leads immediately to the result:

$$Y = \frac{2\alpha\beta n\pi mk}{n^2\pi^2 + \beta^2 q_e k^2 m^2} P. \quad \text{(C7)}$$

Hence, substituting in the linearized evolution equation for the potential perturbation (C5), this is reduced to the following ordinary differential equation with space–time-dependent coefficients:

$$\left\{n^2\pi^2\frac{dP}{dt} + \frac{2\alpha\beta^2 q_e n^2\pi^2 m^2 k^2}{n^2\pi^2 + \beta^2 q_e k^2 m^2} P\right\}(1 - \beta^2\phi_{xx}) + \phi_{zz}\left\{\frac{d(\beta^2 k^2 m^2 P)}{dt} - \frac{2a\beta^2 n^2\pi^2 m^2 k^2}{n^2\pi^2 + \beta^2 q_e k^2 m^2} P\right\} = 0, \quad \text{(C8)}$$

and rearranging the various terms:

$$\left\{\frac{dP}{dt} + \frac{2\alpha\beta^2 q_e m^2 k^2}{n^2\pi^2 + \beta^2 q_e k^2 m^2} P\right\} \times \{n^2\pi^2(1 - \beta^2\phi_{xx}) + \beta^2 k^2 m^2\phi_{zz}\} = 0. \quad \text{(C9)}$$

Provided that the terms in the second parentheses do not cancel each other, and given the initial condition $P(\beta = \beta_0) = P_0$, the following solution is finally obtained:

$$P = \frac{1}{n^2\pi^2 + \beta^2 q_e k^2 m^2}(n^2\pi^2 + \beta_0^2 q_e k^2 m^2) P_0, \quad \text{(C10)}$$

$$Y = \frac{2\alpha\beta n\pi mk}{(n^2\pi^2 + \beta^2 q_e k^2 m)^2}(n^2\pi^2 + \beta_0^2 q_e k^2 m^2) P_0. \quad \text{(C11)}$$

As was expected, the geopotential perturbation P decays in time for positive values of the equivalent potential vorticity q_e, while it grows for negative values of the same parameter. It is observed (Fig. A1) that, in the case of negative equivalent potential vorticity, the growth rate of the potential perturbations increases for increasing wavenumbers in the horizontal direction (m) and for decreasing wave numbers in the vertical direction (n). Furthermore, it reaches an infinite rate, for a given pair of wavenumbers (m, n), at the time when $\beta = (np)/(|q_e|^{1/2}km)$. Such singular behavior

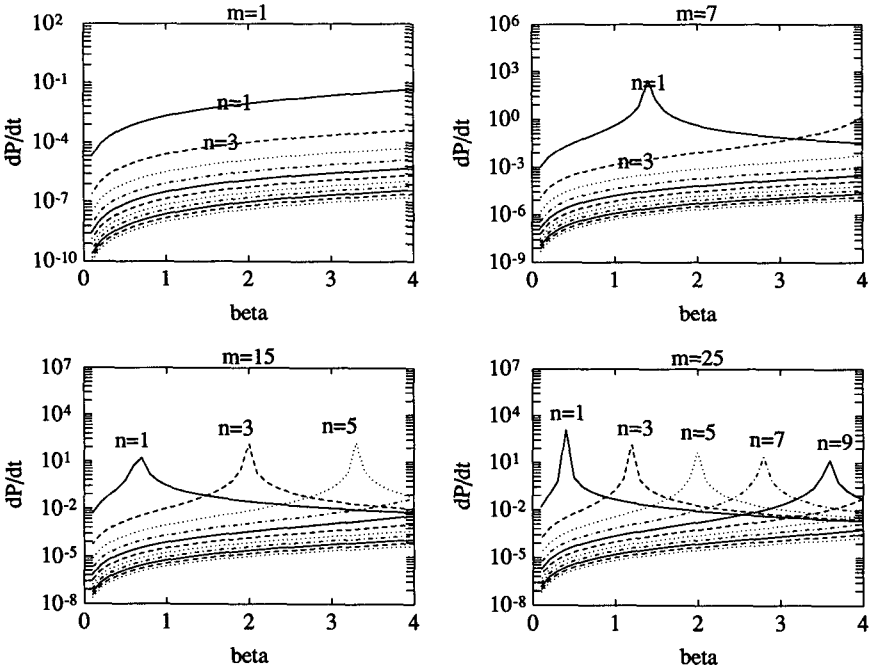

FIG. A2. Temporal evolution of the growth rate (in logarithmic scale) of periodic infinitesimal potential perturbations in a conditionally unstable atmosphere ($q_e = -0.1$), for various wavenumbers in the horizontal (m) and vertical (n) directions.

may be due to the neglect of the inertial terms, in the semigeostrophic approximation, connected to the cross-front velocity. This consideration is supported from the graphs shown in Fig. A2, where the cuspids in the curves represent approximately, for given wavenumbers, the times when the perturbation growth rate goes to infinity. The perturbation "blowup" occurs, before the time of the front formation, only for large horizontal wavenumbers, which represent modes lying far beyond the range of validity of the semigeostrophic approximation. Finally, we note how no explicit interaction is found between the growing instabilities and the base frontal circulation, when the perturbations are taken as periodic in the semigeostrophic space. Such an interaction is implicit in the back-transformation to physical coordinates, which depends on both the base-state geopotential and its perturbations.

REFERENCES

Bennets, D. A., and J. C. Sharp, 1982: The relevance of conditional symmetric instability to the prediction of mesoscale frontal rainbands. *Quart. J. Roy. Meteor. Soc.*, **108,** 595–602.

Blumen, W., 1980: A comparison between the Hoskins–Bretherton model of frontogenesis and the analysis of an intense surface frontal zone. *J. Atmos. Sci.*, **37,** 64–77.

Emanuel, K. A., 1983: Conditional symmetric instability: A theory for rainbands within extratropical cyclones. *Mesoscale Meteorology—Theories, Observations and Models.* D. Reidel, 231–245.

——, 1985: Frontal circulations in the presence of small moist symmetric stability. *J. Atmos. Sci.*, **42,** 1062–1071.

——, and M. Fantini, 1987: Baroclinic instability in an environment of small stability to slantwise moist convection. Part I: Two-dimensional models. *J. Atmos. Sci.*, **44,** 1559–1573.

Hoskins, B. J., 1982: The mathematical theory of frontogenesis. *Ann. Rev. Fluid Mech.*, **14,** 131–151.

——, and F. P. Bretherton, 1972: Atmospheric frontogenesis models: Mathematical formulation and solution. *J. Atmos. Sci.*, **29,** 11–37.

Joly, A., and A. J. Thorpe, 1989: Warm and occluded fronts in two-dimensional moist baroclinic instability. *Quart. J. Roy. Meteor. Soc.*, **115,** 513–534.

Ogura, Y., and D. Portis, 1982: Structure of the cold front observed in SESAME-AVE III and its comparison with the Hoskins–Bretherton frontogenesis model. *J. Atmos. Sci.*, **39,** 2773–2792.

Sanders, F., and L. F. Bosart, 1985: Mesoscale structure in the megalopolitan snowstorm of 11–12 February 1983, Part I: Frontogenetical forcing and symmetric instability. *J. Atmos. Sci.*, **42,** 1050–1061.

Thorpe, A. J., and K. A. Emanuel, 1985: Frontogenesis in the presence of small stability to slantwise convection. *J. Atmos. Sci.*, **42,** 1809–1824.

Xu, Q., 1989: Frontal circulations in the presence of small viscous moist symmetric stability and weak forcing. *Quart. J. Roy. Meteor. Soc.*, **115,**